Chapter 3

OBSERVATIONS AND DATA ANALYSIS

3.1 Observations

Observations were made on two HII regions, Trifid nebula , ($\alpha(1950) = 17^h58^m9^s$, $\delta(1950) = 23^o2'$) (May 21, 1990) and Orion nebula ($\alpha(1950) = 5^h\,32^m\,54^s$, δ (1950) $= -5^o\,25'$) (February 1 to 5, 1992) at Gurushikhar, Mt.Abu. The instrument, namely, the Imaging Fabry-Perot spectrometer (IFPS) was attached at the $f/11$ Cassegrain focus of the 14" C-14 Celestron telescope. A justification for the use of a small-sized telescope is in order. According to the optical extension conservation principle, the product of the area of the telescope primary and the solid angle subtended at the aperture ($S \times \Omega$) should remain constant. For a small telescope, therefore, the loss in collecting area will be exactly compensated by the increase in the observed

angular field. Since our aim is to make observations of an extended region in the HII regions, this trade off between higher spatial resolution in favour of the large field of view is justified. Besides, the non-availability of sufficient amount of observation time on large telescopes due to weather related problems also force us to forgo the possible spatial resolution permitted by the atmospheric seeing, viz. 1 or 2 arc sec. Table 3.1 gives some physical parameters on some well known HII regions.

The following section gives details of the observations made on the two HII regions and the method of data analysis.

3.1.1 Orion Nebula

Orion Nebula (M42; NGC 1976) is the nearest HII region and as such has attracted the attention of observers in the past as well as in the present. It offers a veritable testing ground for various theoretical mechanisms proposed to understand the physics of HII regions. Interferograms were obtained on the Orion Nebula in the emission line of [OIII] 5007 Å centred around the trapezium stars (θ^1 Ori). Scanning of the etalon ET50 (Table 2.1) is done by changing the plate spacing in equal increments and thirty three interferograms were obtained covering about 1.55 Å, one FSR corresponding to 3 Å. We could not cover the entire FSR due to bad weather. The spectral resolution was 6 km/s with an accuracy of 2 km/s in velocity and spatial resolution was 4 arc sec with a field of view of 10.5 arc min. Interferograms

Table 3.1: Properties of five typical HII regions (adopted from Eric Chaisson and extended)

Name of Nebula	Messier Number	position α h m δ o ′	Constellation	m_v†	Diameter arc min(pc)	Distance pc	r_o‡ pc	n_e§ cm^{-3}	Mass $M_\odot$	Electron Temp. K	Turbulent velocity km/s	H_e^+/H^+ %
Orion	M42	05 32.9 -05 25	Orion	4.0	35(5)	460	0.3	2,000	10	9,000	10	9
Trifid	M20	17 58.9 -23 02	Sagittarius	8.5	15(4)	1994	2.5	100	150	8,200	7	10
Lagoon	M8	18 01.6 -24 20	Sagittarius	5.8	25(9)	1074	1.2	400	60	7,500	9	9
Eagle	M16	18 16.0 -13 48	Serpens	6.4	12(6)	2454	3.7	100	600	8,000	12	6
Omega	M17	18 18.0 -16 12	Sagittarius	7.0	20(9)	2147	1.5	800	300	8,700	17	10

†integrated
‡Stromgren Radius
§electron density

were also obtained from a zinc spectral lamp on the ZnI line at the wavelength of 4680.14 Å for calibration purpose in order to (i)check the stability of the instrument during observations and (ii)to obtain the standard radii of the fringes at that line. Fig. 3.1 shows a photograph of Orion Nebula (taken from Shu, 1974).

3.1.2 Trifid Nebula

Trifid nebula (M20; NGC 6514) stands out as the brightest after Orion nebula and the most symmetric HII region observed ever inspite of the three spectacular dust lanes overshadowing its glory. It is classified as an emission and reflection nebula in Sagittarius. A single interferogram was obtained in [OIII] 5007 Å line using an optically contacted etalon with a FSR of 1.25 Å ($\sim$ 75 km/s at 5007 Å). Integration time was 20 minutes. The field of view covered was $\sim 24'$ giving a sky angle of $\sim 4.6''$/pixel on the IPD. Fig. 3.2 shows the Trifid nebula. We could not carry out the scanning at that time as we had used the optically contacted etalon which involves cumbersome pressure scanning. Our attempts later, on large telescopes, using piezo scanned etalons met with little success due to bad weather condition. Nevertheless, the interferogram obtained by us earlier contained considerable information; and to our knowledge it is the first ever interferogram covering such a large region in this nebula.

Figure 3.1: The Orion nebula (from Shu, 1974)

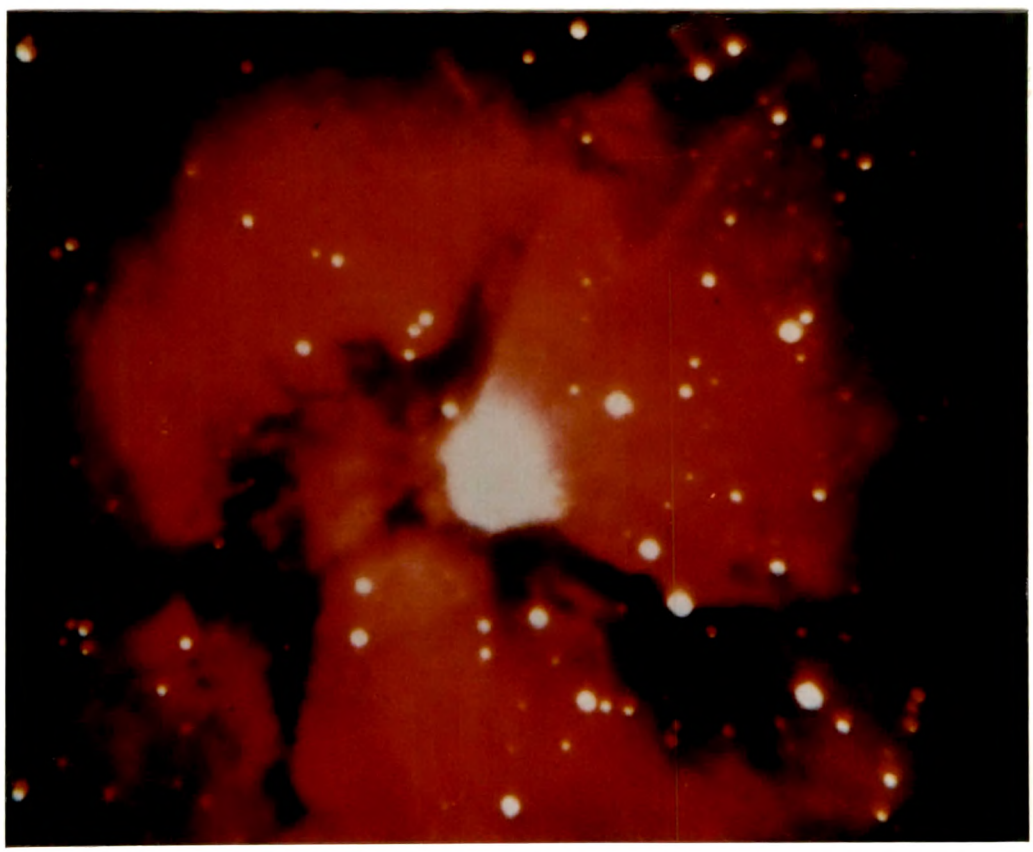

Figure 3.2: The Trifid nebula obtained by combining images in blue, green, and red filters (from Rudolph, 1988)

3.2 Data analysis of the FP interferogram images

The imaging data acquired is in digital (binary) form: ten bits of X and ten bits of Y with 512×512 pixels with the intensity at each position given by 16 bits.

3.2.1 Smoothing the data

A set of softwares were written to extract the kinematic information from the interferograms. Firstly the images are smoothed for random statistical noise by using a 3×3 convolution matrix

$$\begin{bmatrix} -1 & -1 & -1 \\ -1 & -1 & -1 \\ -1 & -1 & -1 \end{bmatrix}$$

This process essentially averages the counts of nine pixels in an array of [3 × 3] and assigns the resulting number to the central pixel. The next step in the process of data analysis is to find the exact coordinate of the centre of the standard source interferogram. For this, an approximate centre is obtained by reading the [X,Y] coordinates from the screen of the VGA monitor. A software is developed and used to find the maximum intensity points cutting across the fringes by searching along the radius vectors starting from the approximate centre of the interferogram in all directions (0°to 360°) by adding the data points in a sector of 5° to increase the signal to noise ratio. Using these maximum intensity points, the equation of circle is fitted by the

method of least squares. Thus in the general equation of a circle,

$$x^2 + y^2 + 2gx + 2fy + c = 0$$

where g, f and c are constants, the position $(-g, -f)$ gives the actual centre of the interferogram. The radius of each fringe of the standard interferogram is thus obtained.

3.2.2 Calibration

The purpose of the standard interferogram is to calibrate the fringe constant involving the focal length of the camera or imaging lens f_{cam} and the gap of the etalon, t. Usually these two parameters are supplied by the manufacturer. However, small errors in these might lead to systematic errors in the fringe positions.

From eqn. 2.1, we get for central fringe,

$$2\mu t = n_o \lambda$$

for p^{th} fringe

$$2\mu t cos\theta_p = n_p \lambda$$

Subtracting the two equations, we get

$$2\mu t(1 - cos\theta_p) = (n_o - n_p)\lambda$$

θ being small, we can write this as

$$\mu t\theta_p^2 = (n_o - n_p)\lambda$$

For air gap μ=1; and writing $(n_o - n_p)\lambda$=pλ and $\theta_p = r_p/f_{cam}$

Therefore,

$$tr_p^2/f_{cam}^2 = p\lambda$$

$$r_p^2 = \frac{f_{cam}^2 p\lambda}{t} + c \tag{3.1}$$

where c is a constant which accounts for the fractional order and r_p is the radius of the p^{th} ring. The plot of r_p^2 vs p (Fig. 3.3) gives a straight line with slope or the fringe constant

$$m = \lambda f_{cam}^2/t$$

From this we can obtain,

$$f_{cam} = \sqrt{\frac{t \times m}{\lambda}} \tag{3.2}$$

and the effective focal length of the camera lens can thus be obtained.

The calibration fringes were obtained at three different positions of the etalon spacing, one in the beginning of the scan (step 1), one in the middle (step 15) and one in the end (step 33).

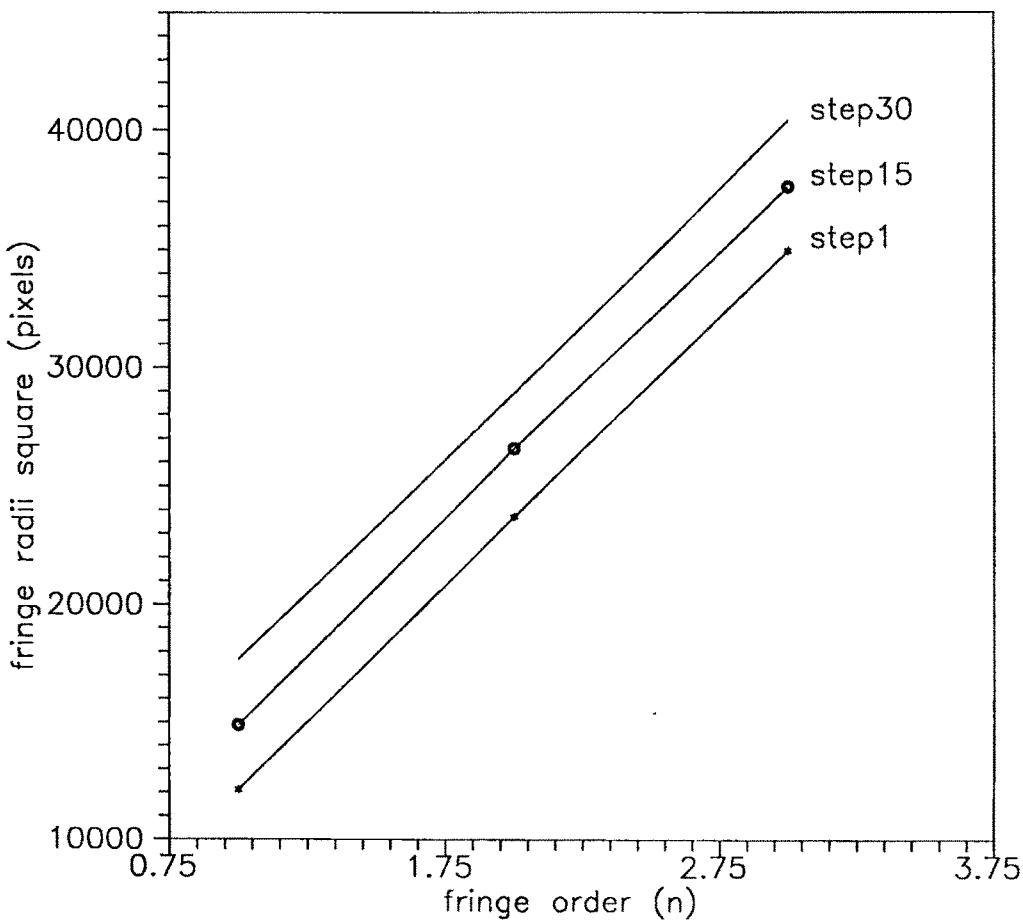

Figure 3.3: Radius square versus order of fringe

The slope m and intercept c at these positions are found from the Fig. 3.3 and used to calibrate the slopes and intercepts of the intermediate fringes. The value of $t(gap)$ at each step is evaluated then. This is done by first finding the number of steps to scan one free spectral range of the etalon. In order to scan the etalon (ET50) by one FSR (3 Å) at λ 5007 Å we need to change the gap t by $\lambda/2$ (=2503.5 Å). This was done in about 64 steps with each step corresponding to a change in t of about 39 Å . Thus after the first stage, the plate separation corresponds to $t = t_o + 39$Å , where t_o is the initial gap. Substituting the values of m, c and t in eqn. 3.1, the corresponding values of radii of fringes are obtained at each value of the gap/separation of the etalon plates.

3.2.3 Determination of line of sight or radial velocities

Any deviation in the line-of-sight or radial velocity at any point on the sky due to the kinematics of the nebula changes the shape and position of the object fringes in comparison to the standard fringes. Thus a redward shift in velocity will result in contraction whereas a blueward shift will result in expansion of the fringes. A software is developed and used to first scan the object interferograms starting from the proper centre radially in all directions and adding the photon counts in a sector of 5° in order to improve upon the S/N ratio. From the constructive interference condition, for i^{th} fringe,

$$2\mu t cos\theta_i = n\lambda$$

and since $\tan\theta_i \sim \theta_i \sim r_i/f_{cam}$, we get,

$$r_i{}^2 = 2f_{cam}^2 - \frac{f_{cam}^2 n\lambda}{\mu t}$$

The difference of the squares of radii of two adjacent fringes is thus given as

$$r_{i+1}{}^2 - r_i{}^2 = \frac{f^2\lambda}{\mu t}$$

which is a constant. The difference between radii of adjacent fringes corresponds to the free spectral range of the FP. This gives the calibration factor for converting the radii into wavelength units. Since the standard fringes are obtained in the zinc line at $\lambda = 4680.14$ Å , corresponding correction factor is applied for the observed wavelength λ =5007 Å . The shift in wavelength ($\Delta\lambda$) from the standard line is then obtained. Finally from the Doppler shift formula

$$v/c = \Delta\lambda/\lambda$$

the relative radial velocities are calculated.

It should be mentioned here that the radial velocities obtained are not absolute values but are only relative. However, this will not affect the understanding of the internal kinematics of the nebula, since we consider only the difference in the radial velocities on the nebula with reference to a fixed point on it.

Radial velocity profiles are generated for more than 2000 positions on the Orion nebula. In general, the profiles looked asymmetric and broad-

winged which necessitated us to resolve them into the constituent gaussian profiles. The profile at each position is fitted by the appropriate number of gaussians (usually and in most cases two) using a multigaussian fitting package (Anandarao and Suhasini Rao, 1985) to obtain the peak position, FWHM and amplitude of the individual gaussian components of the composite fringe profile at any given position. Quite obviously, any multigaussian fitting software cannot give unique results. However, in some cases atleast, prior information about the object would be of great help in order to check the meaningfulness of the solution. Analysis of the data is done for two types of studies: (i) involving general velocity pattern in which the relative velocities so obtained are mapped to get iso-velocity contour maps. The contours are generated using a readymade software package 'Surfer'available on IBM-PC (Golden softwares) and (ii)statistical analysis to study the fluctuations of velocities in a turbulent H II region. The spatial resolution ($\approx$ 2 pixels) in our observations on Orion nebula is about 4 seconds of arc which corresponds to a distance scale of 0.0087 pc while in the case of Trifid, it is about 9.2 seconds of arc corresponding to 0.0058 pc.

3.2.4 Errors in data reduction

The errors involved are of two types (i) systematic errors and (ii) random errors. The following section gives the details of the errors and their estimates.

Systematic errors

The main source of error is due to the instability of the FP etalons. The plate parallelism of the FP etalons is maintained by the servo-control system which utilizes a ceramic reference capacitor. There is a possibility that the value of the capacitance is changed due to change in any one of the physical environmental parameters, viz. pressure, temperature and humidity. This will be reflected in the line profile of the instrument which shows a drift in the peak position. Therefore, to keep a check on such spurious changes, calibration scans are taken from a standard spectral lamp several times during the course of the observations. It has being verified in the case of central spot scanning method that during a scan of about 3 minutes duration, for one order of sampling with 200 sampling points, the departure was 0.015 km/s (Banerjee, 1990). Further, the FP resolution $\delta\lambda$ is 0.1 Å which corresponds to about 6 km/s. This reflects an error in the profile widths of about 3.3 km/s. The velocity position errors (in radial velocities) corresponds to about 2 km/s.

Random errors

In any photon counting device, the S/N ratio depends on the statistical fluctuations in the incident beam of photons. The Poisson distribution is a good approximation of these fluctuations. Therefore, if g represents the average number of photon events in a unit interval of time, the probability of

observing k counts in that particular time interval is given as (Young, 1974)

$$P_g(k) = \frac{g^k e^{-g}}{k!}$$

The standard deviation (i.e., noise) of this distribution is given as $\sqrt{g}$.

Therefore,

$$S/N = g/\sqrt{g} = \sqrt{g}$$

In the present high-resolution spectroscopic observations, the noise is mainly detector-limited as the sky noise can be neglected in most cases. The dark noise over the entire surface of the detector was found to be about 300 counts/s at 20°C.

Errors in Data reduction

The line profiles are fitted with the appropriate gaussians using the multi-gaussian fitting package. But the solution is not unique and it is possible to make two different fits with a different set of the parameters (amplitudes, position and FWHM). It is found that this will involve basically an error in the estimation of amplitude, peak position, half-width values of about 10%. The searching and locating of the intensity maxima and finding the exact centre of the interferogram by the least square method results in an error of approximately $\pm$ 1 pixel which corresponds to an error in Doppler velocities of $\pm$ 2 km/s.